Optimal constant acceleration motion primitives

Gregor Klančar and Sašo Blažič

***Abstract*—This article proposes new motion primitives that are time-optimal and feasible for a vehicle (wheeled-mobile robot). They are parameterized by a constant acceleration and a constant deceleration in an obstacle-free environment between an initial and a final configuration with given poses and velocities. The derived compact parametric solution has implicit optimal velocity profile, is continuous in C^2, considers driving constraints and is computationally efficient. The path is derived analytically considering constraints on maximal allowable driving velocity and accelerations. The obtained motion primitives have continuous transition of curvature and are thus easily drivable by the vehicle.**

The proposed motion primitives are evaluated on several path-planning examples and obtained solutions are compared to a numerically expensive planner using Bernstein-Bézier (BB) curve with path shape and velocity profile optimization. Numerous experiments have been conducted not only in the simulation environment but also during testing and comparisons on the actual mobile robot platforms. It is shown that the proposed solution is computationally efficient, time optimal under given constraints and trapezoidal velocity profile assumptions and is close to globally optimal solution with an arbitrary velocity profile.

***Index Terms*—Path planning, motion primitives, minimal time, driving constraints.**

I. Introduction

Path planning is a fundamental task of any autonomous mobile vehicle and has been extensively studied in the literature. The majority of existing path planners provide solutions described by a set of way-points [1], [2]. Such a path is often not feasible and may result in control tracking errors and uncomfortable driving due to sudden acceleration changes involved [3]. Although such simple solutions might be sufficient for several applications, this is not desired in performance demanding applications where comfortable driving (e.g. wheelchairs or self-driving cars), minimal-time driving or low actuator wear for robust long-time performance is preferred [4], [5]. To obtain semi feasible paths (e.g. with smooth velocities or curvature) in obstructed environments usually a fixed set of motion primitives is used to build a state lattice graph where path is searched [2], [6], [7]. Obtained paths minimize defined criteria, e.g., minimal distance, maximal clearance, energy or similar in the applied space discretization. However, finding globally minimal-time solutions or at lest sufficient approximations with a numeric search is computationally too expensive.

Shortest path planning in obstacle free environment has achieved wide attention. The first works on shortest paths for curvature-constrained vehicles are done by [8], [9] and [1]. An optimal control law that steers the robot on a shortest distance to the goal is provided in [10]. Shortest paths study for wheeled robots with field-of-view constraints has been reported in [11]. Recently, also minimal energy path planing has drawn considerable attention to maximize mobile robot performance considering its limited on-board power [12], [13].

However, similar application of feasible minimal-time path planning to wheeled mobile robots are rare. More common are non-smooth (with discontinuity in curvature or orientation) planning approaches resulting in minimal distance or minimal time paths; or smooth planners which are not optimal in the sense of distance or time. Besides circular arcs and straight motion also several smooth motion primitives applicable in path planning or path smoothing were suggested, such as Bezier curves [2], [14], clothoids [15], higher order polynomials [16] and eta-spline motion primitives with continuous accelerations [4], [17]. Some approaches apply path-velocity decomposition to compute admissible velocity profile that minimize time on a predefined path [18]–[21].

Time-optimal trajectory planning considering bounded velocities of the differential drive's wheels which can be discontinuous is proposed in [22]. Minimal-time trajectory for a robot with bounded acceleration where at least five switched sequences are applied in bang- bang control is proposed in [23]. A geometric reasoning is applied by [24] to obtain time-optimal trajectories for bidirectional steered robot. Such minimal-time path planners usually assume unobstructed environments and find a trajectory between the given initial and the final configuration. As shown in [25] maximal-acceleration bang-bang trajectories obtained numerically following Pontryagin's maximum principle are time-optimal candidates. But due to increased complexity of multiple DOF, minimal-time solutions quickly become too complex to be solved analytically.

This article addresses optimal time trajectory planning for a wheeled vehicle in a free space with given initial and final poses and velocities and considering constraints on velocity and acceleration. In the similar existing works [22]–[25] the necessary conditions for existence of the globally time-optimal trajectories are given which combine several controls that are either wheel's maximal velocities [22], or wheel's maximal accelerations [23], [25], or turning radii [24]. The obtained trajectories do not have continuous curvature and describes the trajectory as a sequence of discontinuous controls. Our approach assumes single switch from constant-accelerated to constant-decelerated (CACD) motion restricted by a slip-free-driving requirement and derives the time-optimal solution considering those assumptions. The obtained optimal trajectory is a parametric function of the two accelerations and it has continuous curvature. The main idea is illustrated by the proposed basic solution that considers trapezoidal velocity profile with a constant-acceleration section, a constant-velocity

G. Klančar and S. Blažič are with Faculty of Electrical Engineering, University of Ljubljana, Tržaška 25, SI-1000 Ljubljana, Slovenia e-mail: gregor.klancar@fe.uni-lj.si

section and a constant-deceleration section. Extensions of this basic approach are proposed to obtain solutions where not only the velocity and acceleration are bounded but also continuous curvature of the trajectories is guaranteed.

The obtained minimal time trajectory is a parametric function of time where optimal velocity profile is implicitly defined by the solution. The solution is therefore obtained in one step. No additional velocity optimization is required in the second step as in [18] or [19]. To find the optimal solution only two equations need to be solved for two unknown parameters (constant acceleration and constant deceleration). The solution is found numerically in a bounded space of these two parameters. This lowers the complexity compared to a strictly numeric solution where optimal solution is found by optimization of three or more variables (e.g. maximal velocity) and applying numeric simulations of the vehicle kinematic model to compute robot trajectories in each iteration of the optimization. Thus the obtained solution is computationally efficient and compact. It assumes trapezoidal velocity profile with constant accelerations and bounded maximal velocity and acceleration constraints. It is shown that these assumptions applied in the proposed CACD path planner produces results which are very close to the globally optimal solutions, i.e. the solutions where the path is completely arbitrary. To evaluate and compare results the fifth order Bernstein-Bézier (BB) curve planner is applied with four free parameters defined by optimization of path and velocity profile to minimize the travelling time.

The proposed CACD motion primitives can have several applications. It can be used to smooth robot paths which are defined by a set of straight line segments with discontinuous orientation. Such a path is usually the output of many path planners in environment with known obstacles. Similarly is done in [26], [15] where apply clothoids to obtain necessary conditions for the locally time-optimal smoothing primitives. It can be used to plan trajectories in unobstructed environments from initial to desired final configuration in a smooth and time-optimal fashion. It can also be applied to smooth path planners in obstructed environments to compute cost-to-goal heuristics such as in [5] or to use CACD primitives with continuous transitions of curvature to build a lattice graph for optimal path searching algorithms as in [5]–[7] or in kinodynamic RRT* planners [3], [27], [28].

II. Driving constraints

When searching for the minimal time the main goal of trajectory planing is to compute a path with a velocity profile that is easily drivable by mobile robots and achieves the target pose within a reasonable time. When optimizing driving time a vehicle needs to maximize its velocity v. The maximal velocity v_{MAX} that the vehicle can achieve is always limited in practice. The acceleration (the rate of change of velocity) is also limited not only because of robot capabilities but also to prevent lateral and longitudinal slip. Maximal tangential acceleration imposed by the drive is usually higher than the one required by the slip-free driving. We will therefore concentrate on the acceleration constraints imposed by slipping in the sequel.

Tangential acceleration $a_t = \frac{dv}{dt}$ in a straight motion is constrained by maximal tangential acceleration a_{MAXt} where the torque on the wheels produces the force in the ground contact that is lower or equal to the friction force. When driving on a curved path (with the curvature κ) with a constant tangential velocity v and an angular velocity ω, the radial acceleration $a_r = v\omega = v^2\kappa$ is constrained by maximal radial acceleration a_{MAXr} to have the centrifugal force lower than the wheel lateral friction force. Combining tangential and radial accelerations, slipping is avoided if the radial acceleration and the tangential acceleration are kept inside the ellipse defined by a_{MAXt} and a_{MAXr}:

$$\frac{a_t^2}{a_{\mathrm{MAXt}}^2} + \frac{a_r^2}{a_{\mathrm{MAXr}}^2} \leq 1 \tag{1}$$

Optimality in the sense of driving time therefore requires driving on the boundary of ellipse defined by (1) [18], [19]. When v_{MAX} is achieved, acceleration might not be on the boundary of the ellipse (1) but rather inside of the ellipse.

III. Optimal constant acceleration curves

The idea is to follow similar strategy as the one resulted from by Pontryagin's principle applied on a double integrator. The vehicle applies maximum acceleration for some time and maximum deceleration for some time to reach the desired location. It has been shown in [25] that the trajectories obtained on differential drive using maximal accelerations are time-optimal candidates. Optimality was evaluated using a numeric procedure where robot path was simulated using numeric integration of robot kinematics and numeric examination of identified sets of time-optimal trajectories.

In the proposed approach we derive parametric equations for the optimal-time trajectory analytically and then solve them to compute the required maximal accelerations as follows. Maximal constant acceleration is defined by a point (a_{t1}, a_{r1}) on the ellipse (1) with $a_{t1} > 0$ and maximal deceleration by another point (a_{t2}, a_{r2}) with $a_{t2} < 0$. Without loss of generality[1] let us assume the vehicle is initially located in the origin with its orientation pointing in the direction of x axis ($x_{sp} = y_{sp} = 0$, $\theta_{sp} = 0$), and has velocity v_{sp}, while the desired end pose and velocity are x_{ep}, y_{ep}, θ_{ep}, and v_{ep}, respectively. The main goal is to find such constant acceleration pair (a_{t1}, a_{r1}) and constant deceleration pair (a_{t2}, a_{r2}) to reach the desired end pose within a minimal time which implies that both pairs need to fulfill relation (1).

A. Curve definition

The trajectory obtained during acceleration is defined by tangential velocity $v_1(t) = v_{sp} + a_{t1}t$, angular velocity $\omega_1(t) = \frac{a_{r1}}{v_1(t)} = \frac{a_{r1}}{v_{sp}+a_{t1}t}$ and vehicle's differential drive kinematics

$$\begin{aligned} \dot{x}(t) &= v(t)\cos(\theta(t)) \\ \dot{y}(t) &= v(t)\sin(\theta(t)) \\ \dot{\theta}(t) &= \omega(t) \end{aligned} \tag{2}$$

[1]Such initial condition is easily achieved by a simple affine coordinate transformation.

Note that the approach presented in this paper does not only apply to differentially driven mobile robots but also to a much more general class of wheeled mobile robots whose input commands can be expressed as $u_1 = f(v,\omega)$ and $u_2 = g(v,\omega)$ where $f(\cdot)$ and $g(\cdot)$ are smooth functions of v and ω. For example, in the case of a car-like robot with the front wheel steering angle and velocity commands: $u_2 = \alpha = \arctan\frac{\omega d}{v}$ and $u_1 = v_s = \frac{v}{\cos\alpha}$ where d is the distance between the front and the rear wheels axes while the steering angle is limited due to practical implementation ($|\alpha| < \alpha_{MAX}$). Consequently, the maximal curvature of the path is also limited ($\kappa_{MAX} = \frac{\tan\alpha_{MAX}}{d}$) and the obtained acceleration solutions need to fulfill the curvature constraint in the start pose $\frac{a_{r1}}{v_{sp}^2} \leq \kappa_{MAX}$ and in the end pose $\frac{a_{r2}}{v_{ep}^2} \leq \kappa_{MAX}$.

Considering (2) trajectory during acceleration reads

$$\theta_1(t) = \int_0^t \omega_1(\tau)d\tau = \frac{a_{r1}}{a_{t1}} \ln\frac{v_1(t)}{v_{sp}} \tag{3}$$

$$\begin{aligned} x_1(t) &= \int_0^t v_1(\tau)\cos\theta_1(\tau)d\tau \\ &= \frac{v_1^2(t)\left(2a_{t1}\cos\theta_1(t) + a_{r1}\sin\theta_1(t)\right) - 2a_{t1}v_{sp}^2}{4a_{t1}^2 + a_{r1}^2} \end{aligned} \tag{4}$$

$$\begin{aligned} y_1(t) &= \int_0^t v_1(\tau)\sin\theta_1(\tau)d\tau \\ &= \frac{v_1^2(t)\left(2a_{t1}\sin\theta_1(t) - a_{r1}\cos\theta_1(t)\right) + 2a_{r1}v_{sp}^2}{4a_{t1}^2 + a_{r1}^2} \end{aligned} \tag{5}$$

where $t \in [0, t_1]$, $t_1 = \frac{\hat{v}-v_{sp}}{a_{t1}}$, and $\hat{v} = v_1(t_1)$ is maximal velocity reached at the end of acceleration ($t = t_1$) .

During deceleration ($a_{t2} < 0$, a_{r2}) the vehicle moves from the obtained final pose of the acceleration ($x_1(t_1)$, $y_1(t_1)$, $\theta_1(t_1)$) towards the end pose (x_{ep}, y_{ep}, θ_{ep}). To simplify the derivation of the deceleration part, the obtained trajectory of deceleration (in the sequel denoted as the second part) will be obtained based on the results of accelerated motion from the origin, Eqs. (3), (4), and (5). First, accelerated motion is assumed from the origin with initial velocity v_{ep}, and accelerations $a_{t2}^* = -a_{t2}$, $a_{r2}^* = -a_{r2}$. The following trajectory is obtained:

$$\theta_2^*(t^*) = \frac{a_{r2}^*}{a_{t2}^*} \ln\frac{v_2^*(t^*)}{v_{ep}} \tag{6}$$

$$x_2^*(t^*) = \frac{{v_2^*}^2(t^*)\left(2a_{t2}^*\cos\theta_2^*(t^*) + a_{r2}^*\sin\theta_2^*(t^*)\right) - 2a_{t2}^*v_{ep}^2}{4{a_{t2}^*}^2 + {a_{r2}^*}^2} \tag{7}$$

$$y_2^*(t^*) = \frac{{v_2^*}^2(t^*)\left(2a_{t2}^*\sin\theta_2^*(t^*) - a_{r2}^*\cos\theta_2^*(t^*)\right) + 2a_{r2}^*v_{ep}^2}{4{a_{t2}^*}^2 + {a_{r2}^*}^2} \tag{8}$$

where $t^* \in [0, t_2^*]$ and $t_2^* = \frac{\hat{v}-v_{ep}}{a_{t2}^*}$ to achieve desired velocity $\hat{v}$ at $t^* = t_2^*$.

In the second step the trajectory (6)-(8) is rotated for angle $\theta_{ep} - \pi$ and translated for (x_{ep}, y_{ep}):

$$\begin{aligned} \theta_2(t^*) &= \theta_2^*(t^*) + \theta_{ep} - \pi \\ x_2(t^*) &= x_{ep} - x_2^*(t^*)\cos\theta_{ep} + y_2^*(t^*)\sin\theta_{ep} \\ y_2(t^*) &= y_{ep} - x_2^*(t^*)\sin\theta_{ep} - y_2^*(t^*)\cos\theta_{ep} \end{aligned} \tag{9}$$

The resulting trajectory (9) starts from the end pose in the direction of $\theta_{ep} - \pi$. In the third step, the sense of time is reversed which makes the motion reversed and decelerating (the orientation of the robot therefore changes for $\pm\pi$). This transformation guarantees that the correct final pose and final velocity are achieved.

If proper tangential accelerations a_{t1} and a_{t2} and maximal velocity $\hat{v}$ are chosen, then the ends of the first and the second curve join ($x_2(t_2^*) = x_1(t_1)$, $y_2(t_2^*) = y_1(t_1)$, and $\theta_2(t_2^*) \pm \pi = \theta_1(t_1)$). Note that $\theta_2(t^*)$ is the backward orientation during reversed accelerating driving. To obtain forward direction π is added/subtracted. The overall solution of the joint trajectory is obtained by reversing the time of the second part as follows

$$x(t) = \begin{cases} x_1(t) & 0 \leq t < t_1 \\ x_2(t_2^* + t_1 - t) & t_1 \leq t \leq t_2^* + t_1 \end{cases} \tag{10}$$

$$y(t) = \begin{cases} y_1(t) & 0 \leq t < t_1 \\ y_2(t_2^* + t_1 - t) & t_1 \leq t \leq t_2^* + t_1 \end{cases} \tag{11}$$

B. Minimal time solution

To find optimal solution using constant acceleration and deceleration curve (CACD) one needs to find valid a_{t1}, a_{t2} (according to (1), a_{r1}, a_{r2} are defined) and $\hat{v}$ which minimize the travelling time between given start ($x_{sp} = y_{sp} = 0, \theta_{sp} = 0$, v_{sp}) and desired goal (x_{ep}, y_{ep}, θ_{ep}, v_{ep}).

The solution (a_{t1}, a_{t2}, $\hat{v}$) needs to satisfy the following equality constraints

$$\begin{aligned} \theta_{ep} - \theta_{sp} + 2k\pi &= \theta_1(t_1) - \theta_2^*(t_2^*), \quad k \in \mathbb{Z} \\ x_{ep} &= x_1(t_1) + x_2^*(t_2^*)\cos\theta_{ep} - y_2^*(t_2^*)\sin\theta_{ep} \\ y_{ep} &= y_1(t_1) + x_2^*(t_2^*)\sin\theta_{ep} + y_2^*(t_2^*)\cos\theta_{ep} \end{aligned} \tag{12}$$

which is derived from (9) considering $x_2(t_2^*) = x_1(t_1)$, $y_2(t_2^*) = y_1(t_1)$, $\theta_1(t_1) = \theta_2(t_2^*) + \pi$ and $k \in \mathbb{Z}$. Maximal velocity $\hat{v}$ is defined by the first equation in (12) considering (3) and (6) as follows

$$\Delta\theta = \frac{a_{r2}^*}{a_{t2}^*} \ln\frac{v_{ep}}{v_{sp}} + \left(\frac{a_{r1}}{a_{t1}} - \frac{a_{r2}^*}{a_{t2}^*}\right) \ln\frac{\hat{v}}{v_{sp}} \tag{13}$$

$$\hat{v} = v_{sp} e^{\frac{\Delta\theta - \frac{a_{r2}^*}{a_{t2}^*}\ln\frac{v_{ep}}{v_{sp}}}{\frac{a_{r1}}{a_{t1}} - \frac{a_{r2}^*}{a_{t2}^*}}} \tag{14}$$

where $\Delta\theta = \theta_1(t_1) - \theta_2^*(t_2^*)$. This reduces the number of free parameters from 3 to 2 and therefore simplifies the solution and lowers the computational complexity. To find a solution we thus need to solve only two equations (the second and the third line in Eq. (12)) with two free parameters a_{t1}, a_{t2}^* ($\{a_{t1}, a_{t2}^*\} \in [0, a_{MAXt}]$). Solutions cannot be obtained analytically. However, the numeric solution is easily found because only the bounded space of two parameters needs to be searched on a convex domain as shown in Section III-E. More feasible solutions may exist and therefore minimal

time solution $t_1 + t_2^*$ is defined as a constrained optimization problem (equality constraints are defined by (12)), as follows

$$\begin{cases} \underset{a_{t1}, a_{t2}}{\text{minimize}} \, (t_1 + t_2^*) \\ \text{subject to} \\ \quad x_{ep} - x_1(t_1) - x_2^*(t_2^*)\cos\theta_{ep} + y_2^*(t_2^*)\sin\theta_{ep} = 0 \\ \quad y_{ep} - y_1(t_1) - x_2^*(t_2^*)\sin\theta_{ep} - y_2^*(t_2^*)\cos\theta_{ep} = 0 \end{cases} \tag{15}$$

where the equality constraints define a valid trajectory solution. There can be more solutions because for any given a_{t1}, a_{t2}, the computed radial acceleration can be either positive or negative according to (1) and thus one needs to find solutions for the four possibilities ($a_{r1} > 0, a_{r2} > 0$; $a_{r1} > 0, a_{r2} < 0$; $a_{r1} < 0, a_{r2} > 0$; $a_{r1} < 0, a_{r2} < 0$) yielding different velocities $\hat{v}$ in (14). At the end, the solution resulting in minimal time $(t_1 + t_2^*)$ is selected among these four candidates. Note that at least one of the four possibilities for a_{r1} and a_{r2} always gives a valid trajectory and therefore a minimal time solution of (15) always exists.

An illustrative example is given in Fig. 1 where the start is in the origin, $v_{sp} = 0.8$ ms^{-1}, final pose is $x_{ep} = 0.35$ m, $y_{ep} = 1$ m, $\theta_{ep} = -\pi/4$ and $v_{ep} = 0.5$ ms^{-1}. Maximal accelerations are $a_{MAXt} = 2$ ms^{-2} , $a_{MAXr} = 4$ s^{-2}. Known initial and final velocities define the minimal radii of curvature (black circles in Fig. 1). Minimal time solutions represent three different combinations of radial accelerations while the solution for the fourth combination ($a_{r1} < 0, a_{r2} < 0$) does not exist. The optimal solution of 1.42 s is obtained using $a_{t1} = 0.90$ ms^{-2}, $a_{t2} = -1.14$ ms^{-2}, $a_{r1} > 0$, and $a_{r2} < 0$.

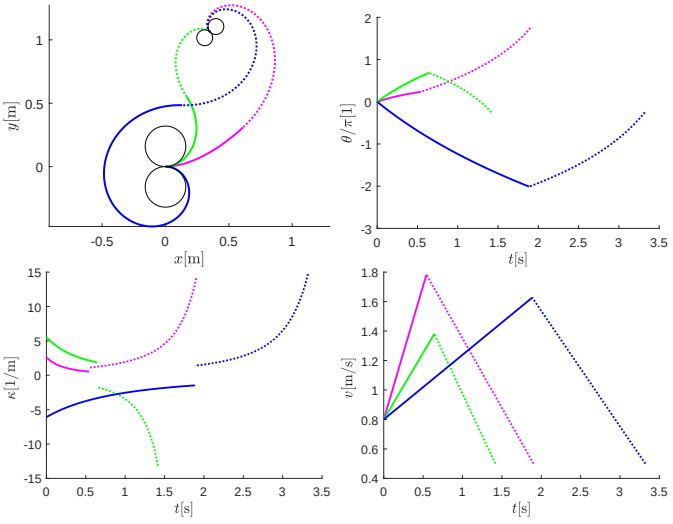

Fig. 1. Shortest time paths using constant accelerations. Shown: path, orientation, curvature, and velocity profile for different radial acceleration combinations. The optimal solution of 1.42 s is obtained using $a_{r1} > 0$, $a_{r2} < 0$.

The obtained solution merely solves two equations for two unknowns and the obtained trajectory has optimal velocity profile. Advantage of the proposed path planner is that the optimal velocity profile does not need to be computed. Instead, it is given implicitly by considered acceleration constraint (1). The solution does not limit tangential velocity which simply is computed so that the vehicle can always accelerate or decelerate. So the vehicle maximal velocity constraints may be violated. Moreover, as seen from Fig. 1, the obtained solution has discontinuous curvature in the point where radial acceleration switches from a_{r1} to a_{r2}. Modifications of this basic solution which improve the mentioned disadvantages are given in the sequel.

C. Modification: velocity constraint

The proposed basic solution can be simply modified by also considering maximal allowable vehicle velocity v_{MAX}. In solutions where the computed $\hat{v}$ exceeds v_{MAX} the driving velocity $v(t)$ is saturated

$$v_s(t) = \begin{cases} v(t) & v(t) \le v_{MAX} \\ v_{MAX} & v(t) > v_{MAX} \end{cases} \tag{16}$$

The vehicle still drives on the same path but it needs more time if velocity is saturated. The time course of the basic trajectory needs to be adapted so that the travelled path will be the same. Whenever $\hat{v} > v_{MAX}$ the velocity saturation starts for acceleration part at $t_{1s} = \frac{v_{MAX} - v_{sp}}{a_{t1}}$ and for deceleration part (reversed acceleration solution) at $t_{2s}^* = \frac{v_{MAX} - v_{ep}}{a_{t2}^*}$. Then the time course given in (10) and (11) needs to be rescheduled as follows

$$t_{sol} = \begin{cases} t & 0 \le t < t_{1s} \\ \frac{s_1(t)}{v_{MAX}} + t_{1s} & t_{1s} \le t < t_1 \\ t_2^* - t^* + \frac{s_1(t)}{v_{MAX}} + t_{1s} & 0 \le t^* < t_{2s}^* \\ \frac{s_2(t_2^*) - s_2(t^*)}{v_{MAX}} + t_2^* - t_{2s}^* + \frac{s_1(t)}{v_{MAX}} + t_{1s} & t_{2s}^* \le t^* \le t_2^* \end{cases} \tag{17}$$

where $s_1(t)$ and $s_2^*(t^*)$ $(t > t_{1s},\ t^* > t_{2s}^*)$ are travelled distances during velocity saturation in acceleration and deceleration part defined by

$$s_1(t) = \frac{(t - t_{1s})(2v_{sp} + a_{t1}t_{1s} + a_{t1}t)}{2}$$

and

$$s_2(t^*) = \frac{(t^* - t_{2s}^*)(2v_{ep} + a_{t2}^*t_{2s}^* + a_{t2}^*t^*)}{2}$$

The solution of the example from Fig. 1 after considering constrained velocity ($v_{MAX} = 1$ ms^{-1}) is given in Fig. 2. The optimal solution of 1.56 s is obtained using $a_{t1} = 0.90$ ms^{-2}, $a_{t2} = -1.14$ ms^{-2}, $a_{r1} > 0$, and $a_{r2} < 0$.

D. Modification: continuous curvature

To make the planned trajectory more appropriate for wheeled vehicles the curvature of the path needs to be continuous in order to prevent sudden jumps of angular velocity while driving. This can be achieved if, besides constant acceleration and deceleration trajectory parts, the trajectory also includes a middle part where the vehicle drives with constant tangential velocity v_L and accelerates only radially so that the curvature changes continuously from the final curvature of the acceleration part to the initial curvature of the deceleration part. If in basic path planning $v(t) > v_{MAX}$, the middle part constant

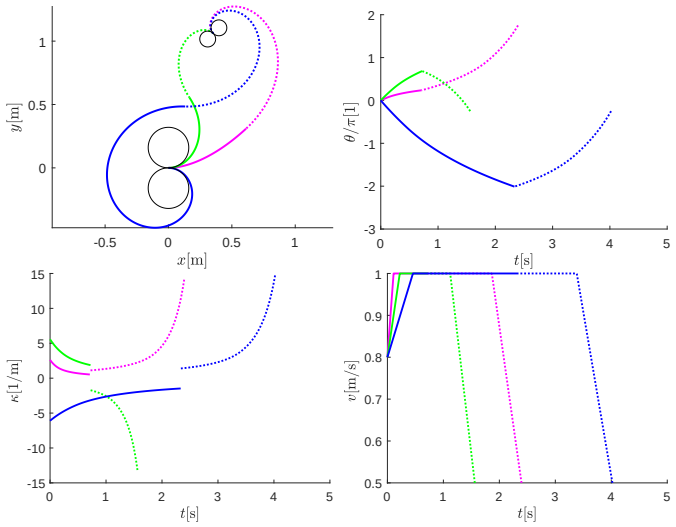

Fig. 2. Shortest time paths using constant accelerations and constrained velocity. Shown: path, orientation, curvature and velocity profile for different radial acceleration combinations. All solutions have longer times according to Fig. 1. The optimal solution of 1.56 s is obtained using $a_{r1} > 0$, and $a_{r2} < 0$.

velocity v_L can be $v_L = v_{MAX}$, otherwise v_L needs to be selected lower than the reached $\hat{v}$ of the basic planning (e.g. $v_L = 0.9\hat{v}$).

Let as assume constant rate of change of radial acceleration during the middle part (the duration of this middle part is Δt which will be given later). Then the radial acceleration of the middle part is defined by

$$a_{r3}(t_3) = a_{r1} + \frac{a_{r2} - a_{r1}}{\Delta t} t_3 \tag{18}$$

where $t_3 \in [0, \Delta t]$ and angular velocity is $\omega_3(t_3) = \frac{a_{r3}(t_3)}{v_L}$. The increment of the orientation made in the middle part is

$$\Delta\theta_3 = \int_0^{\Delta t} \omega_3(\tau) d\tau = \frac{(a_{r1} + a_{r2})\Delta t}{2v_L} \tag{19}$$

This increment of orientation $\Delta\theta_3$ should be included in the orientation condition (the first line in (12)):

$$\Delta\theta_3 = \theta_{ep} - \theta_{sp} - \frac{a_{r1}}{a_{t1}} \ln \frac{v_L}{v_{sp}} + \frac{a^*_{r2}}{a^*_{t2}} \ln \frac{v_L}{v_{ep}} + 2k\pi, \quad k \in \mathbb{Z} \tag{20}$$

taking into account (3) and (6). Considering relation (19), the time of the middle part is defined as

$$\Delta t = \frac{2v_L \Delta\theta_3}{a_{r1} + a_{r2}} \tag{21}$$

The trajectory of the middle part (continuation of the first part) is then given by

$$\theta_3(t_3) = \theta_1(t_1) + \int_0^{t_3} \omega_3(\tau) d\tau = a + bt_3 + ct_3^2 \tag{22}$$

$$x_3(t_3) = x_1(t_1) + v_L \int_0^{t_3} \cos\theta_3(\tau) d\tau \tag{23}$$

$$y_3(t_3) = y_1(t_1) + v_L \int_0^{t_3} \sin\theta_3(\tau) d\tau \tag{24}$$

where $a = \theta_1(t_1)$, $b = \frac{a_{r1}}{v_L}$, $c = \frac{a_{r2} - a_{r1}}{2v_L \Delta t}$, and times of the acceleration part and the deceleration part are $t_1 = \frac{v_L - v_{sp}}{a_{t1}}$ and $t_2^* = \frac{v_L - v_{ep}}{a^*_{t2}}$, respectively. Solutions of (23) and (24) are obtained by Fresnel integrals usually defined by $C(u) = \int_0^u \cos\left(\frac{\pi\tau^2}{2}\right) d\tau$, $S(u) = \int_0^u \sin\left(\frac{\pi\tau^2}{2}\right) d\tau$. Using variable substitution $u = \sqrt{\frac{2c}{\pi}}(\tau + d)$, (23) and (24) can be expressed as follows

$$x_3(t_3) = x_1(t_1) + v_L \sqrt{\frac{\pi}{2c}} \left[\left(C\left(u^+\right) - C\left(u^-\right) \right) \cos f - \left(S\left(u^+\right) - S\left(u^-\right) \right) \sin f \right] \tag{25}$$

$$y_3(t_3) = y_1(t_1) + v_L \sqrt{\frac{\pi}{2c}} \left[\left(S\left(u^+\right) - S\left(u^-\right) \right) \cos f + \left(C\left(u^+\right) - C\left(u^-\right) \right) \sin f \right] \tag{26}$$

where $u^+ = \sqrt{\frac{2c}{\pi}}(t_3 + d)$, $u^- = \sqrt{\frac{2c}{\pi}} d$, $d = \frac{b}{2c}$, and $f = a - cd^2$.

The final trajectory solution consists of acceleration part (Eqs. (3) - (5)), the middle part (Eqs. (22), (25) and (26)) and deceleration part (Eq. (6) - (8)). The solution $\{a_{t1}, a_{t2}\}$ needs to satisfy the following equality constraints (similarly as in (12))

$$\begin{aligned} x_{ep} &= x_3(\Delta t) + x_2^*(t_2^*)\cos\theta_{ep} - y_2^*(t_2^*)\sin\theta_{ep} \\ y_{ep} &= y_3(\Delta t) + x_2^*(t_2^*)\sin\theta_{ep} + y_2^*(t_2^*)\cos\theta_{ep} \end{aligned} \tag{27}$$

where $\theta_{ep} - \theta_{sp} + 2k\pi = \theta_1(t_1) - \theta_2^*(t_2^*) + \Delta\theta_3$. The overall solution is joint trajectory obtained by joining all parts by common time $(x(t_{sol}), y(t_{sol}), \theta(t_{sol}))$

$$t_{sol} = \begin{cases} t & 0 \le t < t_1 \\ t_1 + t_3 & 0 \le t_3 < \Delta t \\ t_2^* - t^* + t_1 + \Delta t & 0 \le t^* \le t_2^* \end{cases} \tag{28}$$

Minimal time solution is then defined as follows

$$\begin{cases} \underset{a_{t1}, a_{t2}}{\text{minimize}} \; (t_1 + t_2^* + \Delta t) \\ \text{subject to} \\ \quad x_{ep} - x_3(\Delta t) - x_2^*(t_2^*)\cos\theta_{ep} + y_2^*(t_2^*)\sin\theta_{ep} = 0 \\ \quad y_{ep} - y_3(\Delta t) - x_2^*(t_2^*)\sin\theta_{ep} - y_2^*(t_2^*)\cos\theta_{ep} = 0 \end{cases} \tag{29}$$

The solution of the example from Fig. 1 which considers maximal driving velocity ($v_{MAX} = 1$ ms^{-1}) and has continuous curvature is given in Fig. 3. The optimal solution of 1.53 s is obtained using $a_{t1} = 0.74$ ms^{-2}, $a_{t2} = -1.11$ ms^{-2}, $a_{r1} > 0$, and $a_{r2} < 0$. The solution results in a bit longer time than the basic solution (Fig. 1) which is due to the velocity constraint. It has lower time than the simple constrained solution (Fig. 2). Due to the middle part, the solution has continuous curvature and is thus easily drivable by a wheeled vehicle. Because of zero tangential acceleration in the middle part the radial acceleration can be higher which allows faster rotation and thus straighter and shorter curves. Consequently, shorter driving times can be achieved in comparison with the simple constrained solution, but the driving time is usually still longer than in the basic (unsaturated) solution because of lower velocities.

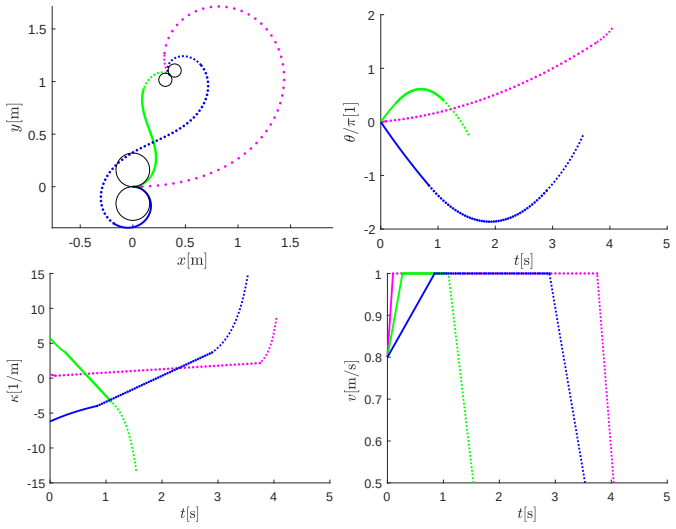

Fig. 3. Continuous curvature shortest time paths using constant accelerations considering constrained velocity. Shown: path, orientation, curvature and velocity profile for different radial acceleration combinations. The optimal solution of 1.53 s is obtained using $a_{r1} > 0$ and $a_{r2} < 0$.

E. Convergence analysis

To answer the question how difficult is to find the solution by optimization, the convergence properties of the algorithm are analyzed. This is done by adopting an unconstrained optimization algorithm (Nelder-Mead simplex direct search method in our case) where the cost function quantifies the squared Euclidean distance D of the equality constraints violation. Equality constraints from (15) are therefore transformed into cost function:

$$D = (x_{ep} - x_1(t_1) - x_2^*(t_2^*)\cos\theta_{ep} + y_2^*(t_2^*)\sin\theta_{ep})^2 + (y_{ep} - y_1(t_1) - x_2^*(t_2^*)\sin\theta_{ep} - y_2^*(t_2^*)\cos\theta_{ep})^2 \quad (30)$$

The proposed CACD solutions will be analysed by showing the cost function D with respect to the free parameters a_{t_1} and a_{t2}. The equality constraints from (15) are satisfied when the cost function (30) becomes zero. There can be several solutions but we are only interested in finding the one that corresponds to the minimum driving time.

Fig. 4 shows the cost function D for the example in Fig. 1 with $a_{r1} > 0$ and $a_{r2} > 0$ (magenta line with travel time 1.9 s in Fig. 1). Only one point ($a_{t1} = 1.81$ ms^{-2}, $a_{t2} = -0.94$ ms^{-2}) satisfies the constraints and its optimal travelling time found using (15) is 1.9 s. Because of convex cost function this solution is found easily.

Fig. 5 shows the quadratic Euclidean distance of constraints violation for the example in Fig. 1 with $a_{r1} > 0$ and $a_{r2} < 0$ (green line in Fig. 1). Here more points satisfy the constraints and they all present valid trajectories, constraint optimization thus returns the one with minimal time which is 1.42 s (at $a_{t1} = 0.90$ ms^{-2}, $a_{t2} = -1.14$ ms^{-2}). In Fig. 5 the optimal solution (fastest trajectory) is marked by a dot. Other valid trajectories (not with minimal time) belong to lower tangential accelerations and higher radial accelerations and can therefore have several encirclement of the start or the end point. Some

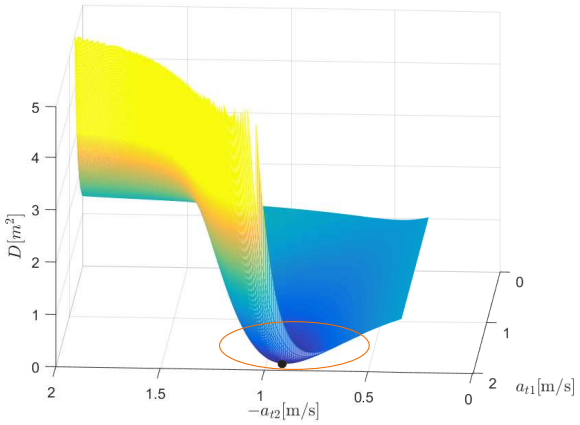

Fig. 4. Squared Euclidean distance of equality constraint violation for $a_{r1} > 0$ and $a_{r2} > 0$ in Fig. 1. Optimal solution of (15) is therefore found at $a_{t1} = 1.81$ ms^{-2}, $a_{t2} = -0.94$ ms^{-2} with travelling time of 1.9 s.

TABLE I
VALID TRAJECTORY'S PARAMETERS AND THEIR TRAVELLING TIMES OBTAINED FOR EXAMPLE IN FIG. 1 WITH $a_{r1} > 0$ AND $a_{r2} < 0$.

time [s]	a_{t1} [ms^{-2}]	$-a_{t2}$ [ms^{-2}]
1.42	0.905	1.137
4.47	0.235	0.403
7.47	0.137	0.246
10.47	0.097	0.177
13.47	0.075	0.138
16.46	0.062	0.110
19.46	0.053	0.091
⋮	⋮	⋮

of those trajectories given in ascending order of the traveling time are given in Table I. The shape of the cost function around all the solutions of the constrained optimization problem (15) is convex but the size of the basin of attraction varies. The cost function around the solutions increases more rapidly for solutions with longer time. The solution with the shortest time (encircled in Fig. 5) has the largest basin of attraction, and therefore it is very easy to be found which is beneficial for the convergence of the proposed algorithm.

IV. Examples and Comparisons

The obtained CACD trajectory, either the basic one (15) or the one with continuous curvature (29), is guaranteed to be time optimal (taking into consideration the given restrictions) as this follows from the problem definition. The obtained trajectory gives the feasible path and at the same time its velocity profile on this path is already time optimal. It is therefore not possible to drive faster on the obtained path if the constraints (on accelerations and maximal velocity) are considered.

A. Comparison with Bernstein-Bézier curve

The remaining question is how close to the global optimum the obtained path is. In other words: can a trajectory with non-constant accelerations which would still obey the mentioned

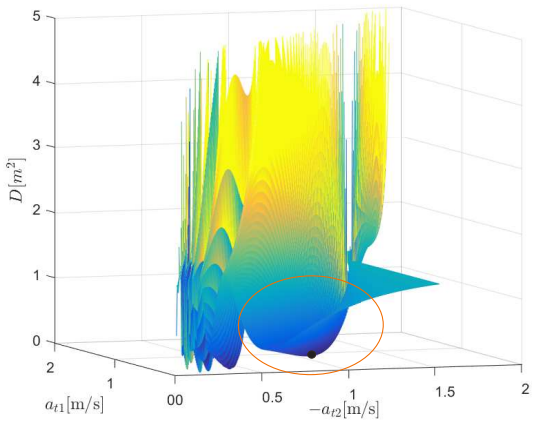

Fig. 5. Squared Euclidean distance of constraints violation for example $a_{r1} > 0$ and $a_{r2} < 0$ in Fig. 1. More parameter sets satisfy the constraints (the distance is zero). Among these, the optimal one found by (15) has the largest convex area (time is 1.42 s, $a_{t1} = 0.90$ ms^{-2}, $a_{t2} = -1.14$ ms^{-2}).

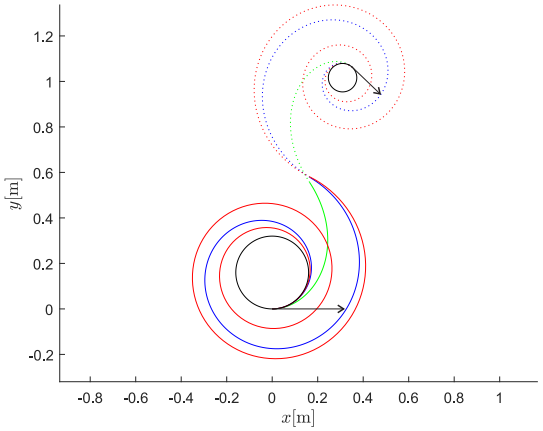

Fig. 6. The first three valid trajectories from Table I for $a_{r1} > 0$ and $a_{r2} < 0$. Valid trajectories with longer times have lower tangential accelerations and higher radial accelerations and therefore have several encirclements of the start or the end point.

constraints be faster? The answer is yes but obtaining such a globally optimal solution would require complex optimization problem and its optimum solution would be quite close to the proposed one. To lower the complexity one therefore needs to reduce the input parameter set (the proposed basic CACD is defined by 2 parameters only). Finding a general globally optimal solution would however require infinite input space (arbitrary continuous curve of acceleration) which is practically impossible to solve.

To illustrate the above statements and evaluate the proposed CACD planner we compare the proposed solution with the optimal solution obtained on a trajectory obtained by fifth order polynomial function described by Bernstein-Bézier (BB) curve

$$\mathbf{r}(\lambda) = (1-\lambda)^5 \mathbf{P}_0 + 5\lambda(1-\lambda)^4 \mathbf{P}_1 + 10\lambda^2(1-\lambda)^3 \mathbf{P}_2 + 10\lambda^3(1-\lambda)^2 \mathbf{P}_3 + 5\lambda^4(1-\lambda)\mathbf{P}_4 + \lambda^5 \mathbf{P}_5 \tag{31}$$

with six control points $\mathbf{P}_i = [x_i, y_i]^T$, $i \in \{0, 1, \cdots, 5\}$ with λ being normalized time ($0 \leq \lambda \leq 1$). BB curve is a parametric

TABLE II
TRAVELLING TIMES COMPARISONS OF THE PROPOSED CACD PLANNER AND THE VELOCITY-OPTIMIZED 4TH AND 5TH ORDER BERNSTEIN-BÉZIER CURVE. DIFFERENT TRAJECTORIES ARE COMPUTED FOR FIXED INITIAL PARAMETERS ($x_{sp} = y_{sp} = 0$, $\theta_{sp} = 0$, $v_{sp} = 0.3$ MS^{-1}, $x_{ep} = y_{ep} = 1$ M, $v_{ep} = 0.5$ MS^{-1}, $v_L = 1.2$ MS^{-1}, $a_{MAXt} = 2$ MS^{-2} AND $a_{MAXr} = 4$ S^{-2}) AND VARYING FINAL ORIENTATION (θ_{ep})

θ_{ep} [°]	t_{CACD} [s]	t_{BB4}[s]	t_{BB5}[s]
-135	2.020	/	/
-90	1.792	/	/
-45	1.614	/	1.572
0	1.507	/	1.492
45	1.475	1.465	1.465
90	1.520	1.494	1.489
135	1.646	/	1.565
180	1.857	/	/
225	2.147	/	/

function where the desired initial and final requirements can be easily set while its shape can be adjusted by free parameters. The first two and the last two control points are defined by the initial and the final conditions as follows: $\mathbf{P}_0 = [x_{sp}, y_{sp}]$, $\mathbf{P}_1 = \mathbf{P}_0 + 0.2 v_{sp} [\cos(\theta_{sp}), \sin(\theta_{sp})]^T$, $\mathbf{P}_5 = [x_{ep}, y_{ep}]$, $\mathbf{P}_4 = \mathbf{P}_5 + 0.2 v_{ep} [\cos(\theta_{ep} + \pi), \sin(\theta_{ep} + \pi)]^T$, and $\mathbf{P}_2$ and $\mathbf{P}_3$ are free control points represented by four parameters which are found by optimization so that the travelling time is minimal. It has to be stressed that the BB curve only defines the path while the optimal velocity profile is computed by numeric integration detailed in [19] and [29] where acceleration constraints (1) are considered. This calculation is performed in every optimization iteration for the obtained BB path.

The comprehensive comparison between the proposed CACD planner and the BB based planner was conducted. Table II shows travelling times for different final poses of the robot. Three algorithms are included: the CACD planner, the 4th order BB planner (two free parameters as in the case of the CACD planner), the 5th order BB planner (four free parameters). We can see that the velocity-optimized BB curve solution improves the travelling time approximately for 1 %. The solution using BB is computationally more intense and its solution is not a parametric function since it includes a nonlinear mapping (numeric look-up table) for obtaining optimal time scheduling ($\lambda(t)$). Notice also that a feasible BB solution cannot be found for cases where higher orientation increments ($\Delta\theta = \theta_{ep} - \theta_{sp}$) are required. This could be improved by increasing the order of the BB curve which increases the degree of freedom and thus approaches the global optimal solution but this also makes the computation time longer.

Fig. 7 shows the comparison of the trajectories obtained by the proposed CACD planner (green curves) and the BB based planner (blue curves). What can be observed immediately is that the BB path is straighter which means that the initial and the final curvature is very large while it is small in the middle part. The final result shows slightly better driving time for the BB curve.

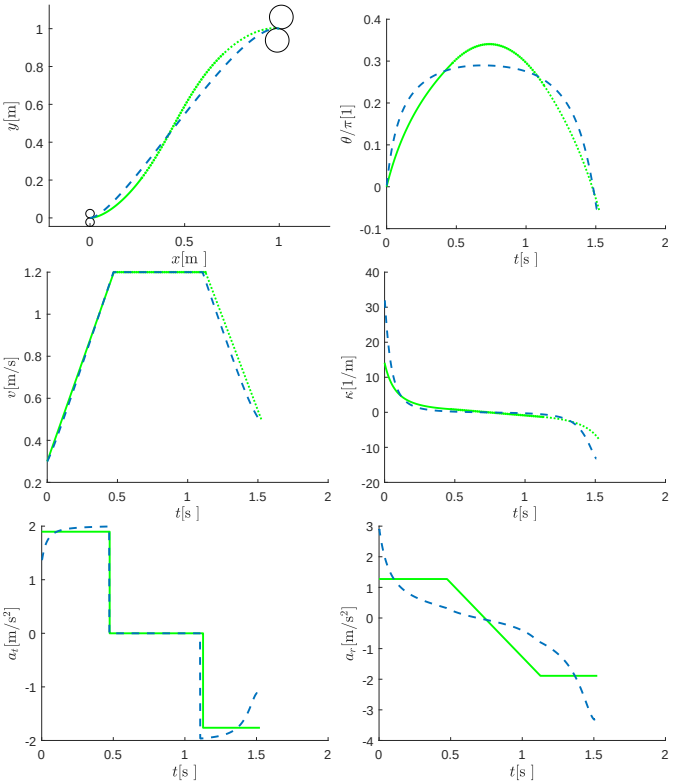

Fig. 7. Comparison of the proposed CACD trajectory (green) and velocity-optimized Bernstein-Bézier curve (blue) for initial parameters ($x_{sp} = y_{sp} = 0$, $\theta_{sp} = 0$, $v_{sp} = 0.3$ ms^{-1}, $x_{ep} = y_{ep} = 1$ m, ,$\theta_{ep} = -10°$, $v_{ep} = 0.5$ ms^{-1}, $v_L = 1.2$ ms^{-1}, $a_{MAXt} = 2$ ms^{-2} and $a_{MAXr} = 4$ s^{-2}).

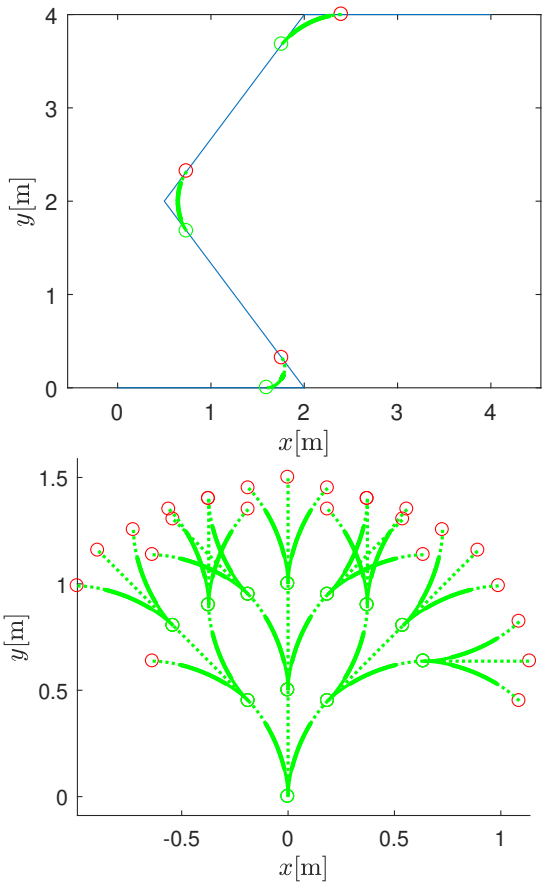

Fig. 8. Illustration of path smoothing application (upper graph) where the straight-line path with discontinuous orientation in the junctions is smoothed by inserting the CACD curves (thick green line). Illustration of a lattice graph construction (lower graph) using CACD motion primitives where each node (final point of the CACD curve) expands to three new vertices connected by the CACD curves.

B. Illustration of other possible applications

The proposed CACD motion planner can have several applications. It can be used as a standalone motion planner in obstacle free environment as illustrated in Sections III and IV-C. It can also be used as CACD motion primitive generator in some other path planners to estimate cost-to-goal heuristics or to build a lattice graph for environments with obstacles. It can as well be used to smooth a path defined by a set of way-points which is obtained from some path planner. Fig. 8 shows an illustration of path smoothing and lattice graph construction. In the upper graph in Fig. 8 the path consisting of straight-line sections (going from $x = 0$ m and $y = 0$ m to $x = 2$ m and $y = 0$ m, then to $x = 0.5$ m and $y = 2$ m, and so on) is smoothed by inserting CACD motion primitives. The start and the goal points of the connecting CACD curve lie at a constant distance from the junction point of the two sequential straight-line segments. The start and the goal orientations are defined by straight-line sections.

The lower graph in Fig. 8 illustrates the lattice graph construction using CACD motion primitives that could be used to explore the environment in some graph-based planner. In this example each CACD curve starts from its parent final pose and ends in the pose with one of the orientation increments $(-45°, 0°, 45°)$.

C. Experiments

Performance of the proposed trajectory planners is checked also by several experiments done on a wheeled mobile robot. The robot (see Fig. 9) has a cube shape with a 7.5 cm side and weighs 0.5 kg. Its pose is estimated with an image sensor and a computer-vision algorithm running at the sampling frequency of 30 Hz. The robot is controlled by commanding its translational velocity ($v(t)$) and its angular velocity ($\omega(t)$) which present the reference for implemented low-level control in the robot.

Trajectory tracking is achieved by nonlinear control law [30]

$$v(t) = v_{ref}(t)\cos e_\theta(t) + k_x(t)e_x(t)$$
$$\omega(t) = \omega_{ref}(t) + k_y(t)v_{ref}(t)\frac{\sin e_\theta(t)}{e_\theta(t)}e_y(t) + k_\theta(t)e_\theta(t)$$

where $e_x(t)$, $e_y(t)$ and $e_\theta(t)$ are the components of the pose tracking error expressed in robot local coordinates, $v_{ref}(t) = \sqrt{\dot{x}^2(t) + \dot{y}^2(t)^2}$ and $\omega_{ref}(t) = \frac{\dot{x}(t)\ddot{y}(t) - \dot{y}(t)\ddot{x}(t)}{\dot{x}^2(t) + \dot{y}^2(t)}$ are the reference velocities computed from the planned trajectory, $k_x(t) = k_\varphi(t) = 2\zeta\sqrt{\omega_{ref}^2(t) + gv_{ref}^2(t)}$ and $k_y(t) = gv_{ref}(t)$ are the controller gains with tuning parameters chosen as $\zeta = 0.8$, $g = 150$.

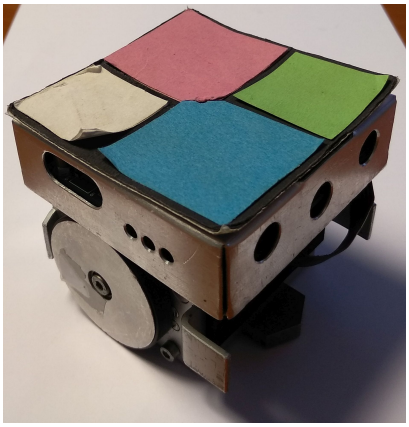

Fig. 9. Robot used during experiments with the color patch used for vision-based localization.

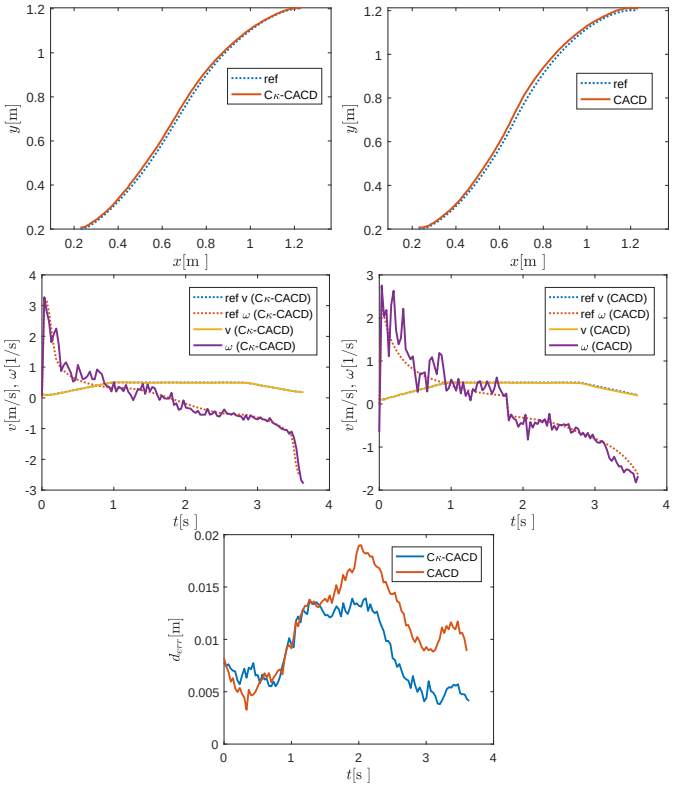

Fig. 10. Comparison of continuous curvature CACD (Cκ-CACD) and basic CACD tracking results. Trajectories parameters are: $x_{sp} = y_{sp} = 0, \theta_{sp} = 0$, $v_{sp} = 0.1$ ms^{-1}, $x_{ep} = 1.3$ m $y_{ep} = 1.2$ m, $\theta_{ep} = -10°$, $v_{ep} = 0.2$ ms^{-1}, $v_L = 0.5$ ms^{-1}, $a_{MAXt} = 0.5$ ms^{-2}, $a_{MAXr} = 0.5$ s^{-2}.

The algorithms treated in this comparison are the basic CACD trajectory planning algorithm with limited maximal velocity (Section III-C) and the CACD trajectory planning algorithm with continuous curvature transitions (Section III-D).

Both planning approaches result in minimal time path under given design constraints (maximal velocity and accelerations). The basic CACD results in an angular velocity with a discontinuity (due to discontinuous curvature). This sudden jump influences the final tracking performance but it can also be hidden by other prevailing effects such as tracking controller dynamics, relatively long sampling time ($T_s = 33$ ms), measurement system delay (in our case approximately $2T_s$ due to localization using image sensor), unmodelled dynamics, wheel sliding and noise.

Experiments on the real mobile robot are shown Fig. 10. The first two plots show the x, y plot together with their references, next two plots show the actual velocities and the commanded velocities while the last plot shows the position error between planned trajectory $(x(t), y(t))$ and robot trajectory $(x_{rob}(t), y_{rob}(t))$ defined as: $d_{err}(t) = \sqrt{(x(t) - x_{rob}(t))^2 + (y(t) - y_{rob}(t))^2}$. In the experiment in Fig. 10 maximal accelerations are selected so the robot can still reliably track the trajectory most of the time. The main purpose of the experiments is to show that both planners can provide similar reference trajectories with similar traveling times ($t_{CACD} = 3.56$ s, $t_{C\kappa-CACD} = 3.63$ s) if observing the paths in Fig. 10. However, due to discontinuity in the curvature present in the basic CACD planner, the required angular velocity needs to make sudden change which causes larger tracking error as seen in Fig. 10. The controller may need some more time to recover from this error if robot is driving with accelerations on the edge of slipping. This effect of discontinuity in curvature becomes noticeable at jump of the angular velocity in the basic CACD (after 1.6 s).

V. Conclusion

In this work, a novel trajectory planning algorithm is proposed to generate minimal time trajectories for wheeled mobile robots. The solution is found for given initial and final configurations considering driving constraints on maximal velocity and accelerations. The proposed solutions are derived analytically for constant-acceleration and constant-deceleration motion. In the basic solution the resulting CACD trajectory is a compact parametric function parametrized by two parameters only, i.e. maximal acceleration and maximal deceleration. These parameters are obtained by constrained optimization which solves two equations for the two unknown parameters. Minimal time solution is easily found as shown in the provided convergence analysis.

To achieve feasible trajectories which vehicles can easily drive on, the basic solution is extended to obtain continuous transitions of curvature. The basic solution and its modification with considered maximal driving velocity (Section III-B and III-C) guarantee optimal trajectory in the sense of traveling time. The solution given in Section III-D results in a continuous curvature trajectory whose traveling time is in the majority of cases even shorter than in solution from Section III-C. This is possible because the inserted path section allows faster robot rotation and consequently straighter and shorter acceleration and deceleration parts. Note that the proposed approach does not only optimize the velocity profile for a given path but instead adapts trajectory to obtain minimal time. This allows to compensate for the lost time due to the included modification by path corrections. The obtained solution is optimal for the defined function in the middle curve part but there may exist a better function.

The proposed solutions are evaluated by several path-planning examples and by a comparison to the planner using

Bernstein-Bezier curves with applied additional velocity optimization. It is shown that CACD planner provides computationally efficient and time optimal solutions using constant-acceleration and constant-deceleration motion and considering the mentioned driving constraints. As such it can be applied in path smoothing and path planning applications as a standalone planner in unobstructed environments or as a motion primitive generator in lattice-graph based search planners in the presence of static or dynamic obstacles.

REFERENCES

[1] T. Fraichard and A. Scheuer, "From reeds and shepp's to continuous-curvature paths," *IEEE Transactions on Robotics*, vol. 20, no. 6, pp. 1025–1035, 2004.

[2] J. Choi and K. Huhtala, "Constrained global path optimization for articulated steering vehicles," *IEEE Transactions on Vehicular Technology*, vol. 65, no. 4, pp. 1868–1879, April 2016.

[3] D. J. Webb and J. van den Berg, "Kinodynamic RRT*: Asymptotically optimal motion planning for robots with linear dynamics," in *2013 IEEE International Conference on Robotics and Automation (ICRA)*, 2013, pp. 5054–5061.

[4] A. Piazzi, C. G. L. Bianco, and M. Romano, " η3-splines for the smooth path generation of wheeled mobile robots," *IEEE Transactions on Robotics*, vol. 3, no. 53, pp. 1089–1095, 2007.

[5] D. Dolgov, S. Thrun, M. Montemerlo, and J. Diebel, "Path planning for autonomous vehicles in unknown semi-structured environments," *The International Journal of Robotics Research*, vol. 29, no. 5, pp. 485–501, 2010.

[6] M. Likhachev and D. Ferguson, "Planning long dynamically-feasible maneuvers for autonomous vehicles," *The International Journal of Robotics Research*, vol. 28, no. 8, pp. 933–945, 2009.

[7] M. Pivtoraiko, R. Knepper, and A. Kelly, " Differentially constrained mobile robot motion planning in state lattices," *Robotics and Autonomous Systems*, vol. 26, no. 3, pp. 308–333, 2009.

[8] L. Dubins, "On curves of minimal length with a constraint on average curvature and with prescribed initial and terminal positions and tangents," *Amer. J. Math.*, vol. 79, pp. 497–516, 1957.

[9] J. A. Reeds and L. A. Shepp, "Optimal paths for a car that goes both forwards and backwards." *Pacific J. Math.*, vol. 145, no. 2, pp. 367–393, 1990.

[10] P. Soueres and J. P. Laumond, "Shortest paths synthesis for a car-like robot," *IEEE Transactions on Automatic Control*, vol. 41, no. 5, pp. 672–688, May 1996.

[11] P. Salaris, D. Fontanelli, L. Pallottino, and A. Bicchi, "Shortest paths for a robot with nonholonomic and field-of-view constraints," *IEEE Transactions on Robotics*, vol. 26, no. 2, pp. 269–281, April 2010.

[12] S. Fallah, B. Yue, O. Vahid-Araghi, and A. Khajepour, "Energy management of planetary rovers using a fast feature-based path planning and hardware-in-the-loop experiments," *IEEE Transactions on Vehicular Technology*, vol. 62, no. 6, pp. 2389–2401, July 2013.

[13] J. Yang, L. Chou, and Y. Chang, "Electric-vehicle navigation system based on power consumption," *IEEE Transactions on Vehicular Technology*, vol. 65, no. 8, pp. 5930–5943, Aug 2016.

[14] J.-W. Choi, R. Curry, and G. Elkaim, *Machine Learning and Systems Engineering*, ser. Lecture Notes in Electrical Engineering 68. Springer Science+Business Media, 2010, ch. Piecewise Bezier Curves Path Planning with Continuous Curvature Constraint for Autonomous Driving, pp. 31–45.

[15] M. Brezak and I. Petrović, "Real-time approximation of clothoids with bounded error for path planning applications," *IEEE Transactions on Robotics*, vol. 30, no. 2, pp. 507–515, April 2014.

[16] B. Sencer, K. Ishizaki, and E. Shamoto, "A curvature optimal sharp corner smoothing algorithm for high-speed feed motion generation of NC systems along linear tool paths," *International Journal of Advanced Manufacturing Technology*, vol. 76, no. 9, pp. 1977–1992, 2015.

[17] F. Ghilardelli, L. Gabriele, and A. Piazzi, "Path Generation Using η4-Splines for a Truck and Trailer Vehicle," *IEEE Transactions on Automation Science and Engineering*, vol. 11, no. 1, pp. 187–203, 2014.

[18] E. Velenis and P. Tsiotras, "Minimum-time travel for a vehicle with acceleration limits: Theoretical analysis and receding-horizon implementation," *Journal of Optimization Theory and Applications*, vol. 138, no. 2, pp. 275–296, Aug 2008.

[19] M. Lepetič, G. Klančar, I. Škrjanc, D. Matko, and B. Potočnik, "Time optimal path planning considering acceleration limits," *Robotics and Autonomous Systems*, vol. 45, pp. 199–210, 2003.

[20] Q.-C. Pham, S. Caron, P. Lertkultanon, and Y. Nakamura, "Admissible velocity propagation: Beyond quasi-static path planning for high-dimensional robots," *The International Journal of Robotics Research*, vol. 36, no. 1, pp. 44–67, 2017.

[21] A. Zdešar and I. Škrjanc, "Optimum velocity profile of multiple bernstein-bezier curves subject to constraints for mobile robots," *ACM Trans. Intell. Syst. Technol.*, vol. 9, no. 5, pp. 56:1–56:23, 2018.

[22] D. J. Balkcom and M. T. Mason, "Time optimal trajectories for bounded velocity differential drive vehicles," *The International Journal of Robotics Research*, vol. 21, no. 3, pp. 199–217, 2002.

[23] M. Renaud and J. Y. Fourquet, "Minimum time motion of a mobile robot with two independent, acceleration-driven wheels," in *Proceedings of International Conference on Robotics and Automation*, vol. 3, 1997, pp. 260–2613.

[24] H. Wang, Y. Chen, and P. Soueres, "A geometric algorithm to compute time-optimal trajectories for a bidirectional steered robot," *IEEE Transactions on Robotics*, vol. 25, no. 2, pp. 399–413, April 2009.

[25] D. B. Reister and F. G. Pin, "Time-optimal trajectories for mobile robots with two independently driven wheels," *The International Journal of Robotics Research*, vol. 13, no. 1, pp. 38–54, 1994.

[26] S. Fleury, P. Soueres, J.-P. Laumond, and R. Chatila, "Primitives for smoothing mobile robot trajectories," *IEEE Transactions on Robotics and Automation*, vol. 11, no. 3, pp. 441–448, 1995.

[27] S. Yoon, D. Lee, J. Jung, and D. H. Shim, "Spline-based RRT* using piecewise continuous collision-checking algorithm for car-like vehicles," *Journal of Intelligent & Robotic Systems*, pp. 1–13, 2017.

[28] G. Tanzmeister, D. Wollherr, and M. Buss, "Grid-based multi-road-course estimation using motion planning," *IEEE Transactions on Vehicular Technology*, vol. 65, no. 4, pp. 1924–1935, April 2016.

[29] G. Klančar, A. Zdešar, S. Blažič, and I. Škrjanc, *Wheeled mobile robotics - From fundamentals towards autonomous systems*. Elsevier, Butterworth-Heinemann, 2017.

[30] C. Samson, "Time-varying Feedback Stabilization of Car-like Wheeled Mobile Robots," *International Journal of Robotics Research*, vol. 12, no. 1, pp. 55–64, 1993.

Gregor Klančar received B.Sc. and Ph.D. degrees in electrical engineering from the University of Ljubljana, Faculty of Electrical Engineering, Slovenia, in 1999 and 2003 respectively.

He is currently an Associate Professor with the Faculty of Electrical Engineering, University of Ljubljana. He lectures autonomous mobile systems at graduate and advanced control of autonomous systems at postgraduate study. His current research interests include autonomous mobile robots, motion control, trajectory tracking, path planning, localization, agent-based behaviour systems and supervision of multiagent systems.

Sašo Blažič received the B.Sc., M. Sc., and Ph. D. degrees in 1996, 1999, and 2002, respectively, from the University of Ljubljana, Faculty of Electrical Engineering, Slovenia.

He is currently a Professor with the University of Ljubljana, Faculty of Electrical Engineering. From 2017, he holds the position of the Vice-Dean for Research at the Faculty of Electrical Engineering, University of Ljubljana. His research interests include adaptive, fuzzy and predictive control of dynamical systems, modelling of nonlinear and evolving systems, autonomous mobile systems, trajectory tracking and path planning of wheeled mobile robots.